Supplementary wavelength calibration methods for SALT/RSS spectropolarimetric observations

Justin Cooper
B.Sc. (Hons)

Submitted in fulfillment of the requirements for the degree
Magister Scientiae
in the Faculty of Natural and Agricultural Sciences
Department of Physics
University of the Free State
South Africa

Date of submission: March 13, 2023

Supervised by: Prof. B. van Soelen, Department of Physics

Abstract

TODO: Done Last... Flow from use of SALT and pipeline and basics of its science implementations into why a more streamlined wavelength calibration is an improvement. Give summary of results. Aim for a paragraph ($\sim$ 600) without going too in-depth into anything specific.

Brian comment: Abstract should summarize paper.Include results, conclusions, etc.

Key words: TODO: Look up keywords for pipeline development and data reduction. I.E. Polarisation: optical, Calibration: wavelength, galaxies: AGN, Blazars, Pipeline, SALT, etc.

Contents

Chapter 1

Introduction

TODO: Very short intro to Spectroscopy, Polarisation, and Spectropolarisation and their Importance in astronomy

TODO: Problem Statement, **VERY IMPORTANT**, roughly a sentence but problem thoroughly fleshed out

Focus on AGN implications and implementations such as the types of objects and a short history for each type of object, Blazar focus with specification on BL Lacs and FSRQs, the Unified Model, ~~The Blazar sequence~~

Brian comment: Highlight importance of polarimetry for understanding emission and how that plays a role in AGN.

Basics of modelling (Different energy/wavelength ranges used and what the models tell us about emission processes/structure) so that Hester's results can be noted for applications of the pipeline.

TODO: General layout of Dissertation

Chapter 2

Spectropolarimetry and the SALT RSS

This chapter gives a brief overview of the basics of spectropolarimetry and how it functions based off of the principles of both spectroscopy and polarimetry. Further, it is discussed how these techniques are practically implemented for South African Large Telescope (SALT), and more specifically the Robert Stobie Spectrograph (RSS), and how the spectropolarimetric reduction process is completed.

2.1 Spectroscopy

Spectroscopy originated in its most basic form with Newton's examinations of sunlight through a prism (Newton and Innys, 1730) but came to prominence as a field of scientific study with Wollaston's improvements to the optics elements (Wollaston, 1802), Fraunhofer's use of a diffraction grating instead of a prism as a dispersion element (der Wissenschaften, 1824), and Bunsen and Kirchoff's classifications of spectral features to their respective chemical elements (Kirchhoff and Bunsen, 1861).

The simplest spectrometer schematic as shown in Figure 2.1 consists of incident light collected from the telescope's optics, labeled A, being focused onto a slit, labeled B, and passed through a collimator, labeled C. The collimator collimates the light allowing a dispersion element (such as a diffraction grating or prism), labeled D, to disperse the light into its constituent wavelengths. The resultant spectrum is focused by a focusing lens, labeled E, onto a focal plane, labeled F. Viewing optics are situated at the focal plane in the case of a spectroscope and a detector is situated at the focal plane in the case of a spectrograph.

The telescope optics refers simply to all the components of a telescope necessary to acquire a focal point where the spectrometer, components labeled B - F, is situated. The focal point in most traditional telescope designs is fixed relative to the telescope and so the spectrometer may be mounted at that point. In cases where the telescope is designed to have a moving focal point relative to the telescope (see Buckley et al., 2006; Cohen, 2009; Ramsey et al., 1998), the spectrometer must also move along the telescope's focal path.

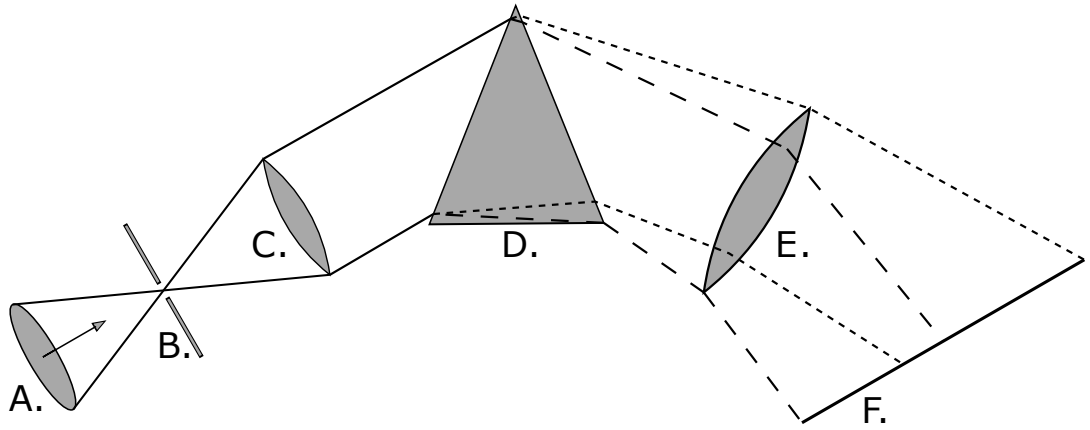

Figure 2.1: Layout depicting the path light collected by a telescope would travel through a simple spectrometer.

The slits function is to control the amount of incident light entering a spectrometer and, along with the exposure time of the detector, prevents over-exposures of bright sources on highly sensitive detectors (Tonkin, 2013). If a source is spatially resolvable, or larger than the seeing conditions, the slit further acts to spatially limit the source to increase the spectral resolution, resulting in sharper features in the resultant spectrum.

Without a slit the spectral resolution would be determined by the projected width of the source on the detector, or the seeing if the source was a star-like point source. Increasing the spectral resolution comes with the trade-off of decreasing the light collected from the source and thus acquiring a less intense resultant spectrum. Multiple spectra may be acquired simultaneously when the slit is positioned such that collinear sources lie along the slit.

The collimating lens functions to collimate the focused light from the telescope, ensuring that all light rays run parallel before reaching the dispersion element. Since the collimator accounts for the telescope's focus, the focal ratio of the collimator, f_1/d_1, should thus optimally match the focal ratio of the telescope, f/D, as seen in Equation 2.1 to be most efficient and to not waste collecting area or material on too large a collimator.

$$\frac{f}{D} = \frac{f_1}{d_1} \tag{2.1}$$

The dispersion element is the element that defines a spectrometer. As the name suggests, a dispersion element disperses the light incident on it into its constituent wavelengths and produces a spectrum. There are two types of dispersion elements, namely the prism and the diffraction grating, which operate on different principles, as discussed in Section 2.1.1.

The focusing lens functions similarly to that of the telescope's optics but in this case focuses the dispersed light onto some receiver situated at the focal plane. As mentioned previously, an eye piece is fixed to the focal point for a spectroscope while a spectrograph employs a detector.

The two most prevalent detector types in spectroscopy are the Charged-Coupled Device (CCD) and Complementary Metal-Oxide-Semiconductor (CMOS) detectors. In astronomical spectroscopy however, sources are fainter and exposure times are much longer

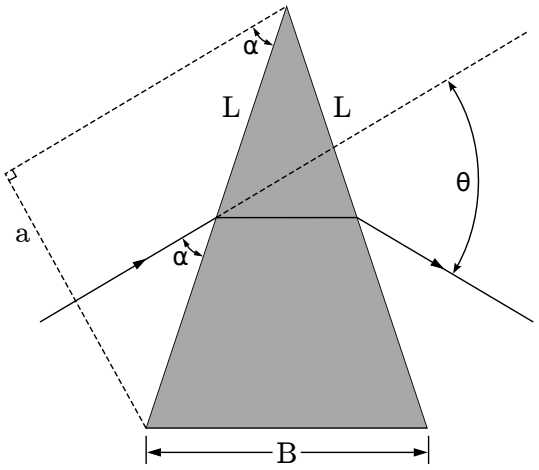

Figure 2.2: Geometry of a prism refracting an incident monochromatic beam at a minimum deviation angle.

and so the CCD detectors are by far the preferred detector as their output has a higher-quality and lower-noise when compared to CMOS cameras under the same conditions (Janesick et al., 2006).

The CCD is a detector composed of many thousands of pixels which can store a charge so long as a voltage is maintained across the pixels. Each pixel detects incoming photons using photo-sensitive capacitors through the photoelectric effect and converts the photons to a charge (Buil, 1991). There are also thermal agitation effects which introduce noise to the charge accumulated by a pixel, further discussed in Section 2.1.2. Once the exposure is finished the accumulated charge is read column by column, row by row, through an Analog-to-Digital Converter (ADC) which produces a two dimensional array of 'counts' with which information may be extracted from. Each CCD image may be referred to by a name such as a bias, dark, flat field, or science image, which helps the observer differentiate the purpose of each image, also further discussed in Section 2.1.2.

2.1.1 Dispersion Elements

Light can be broken up into its constituent wavelengths through two different physical phenomena, namely dispersion and diffraction, which dispersive elements use to create spectra. Dispersive prisms and diffractive gratings each have their strengths and weaknesses and a wide spectrum of instruments exist implementing both, or either, concepts. Regardless of the specific element, dispersive elements all have a resolving power, R, and an angular dispersion. Generally, while the angular dispersion is a more involved process to determine, the resolving power of a spectrograph can be measured as:

$$R = \frac{\lambda}{FWHM} \tag{2.2}$$

where λ is the wavelength of an incident monochromatic beam and $FWHM$ refers to the width of the feature on the detector at half of its maximum intensity.

The prism operates on the principle that the refractive index of light, n, varies as a function of its wavelength, λ. Prisms were the only dispersive elements available for early spectroscopic studies, but they were not without flaw.

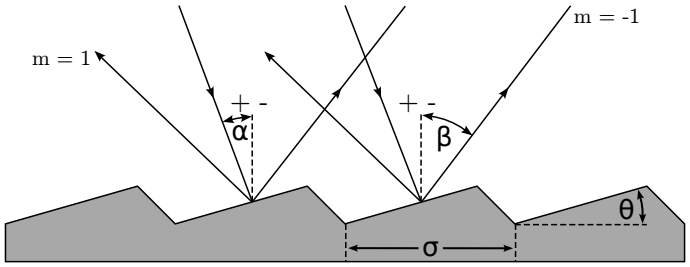

Figure 2.3: Geometry of a reflective blazed grating refracting an incident monochromatic beam

$$\frac{d\theta}{d\lambda} = \frac{B}{a}\frac{dn}{d\lambda} \tag{2.3}$$

The angular dispersion of a prism can be represented by Equation 2.3 where the variables relate to Figure 2.2 such that θ is the angle at which the refracted light differs from the incident light, λ is the wavelength of the incident light, B is the longest distance the beam would travel through the prism, and $a = L\sin(\alpha)$ is the cross-section of the incident beam where L is the length of the transmissive surfaces and α is the incident angle of light to the prism surface. The refractive index of a material as a function of its wavelength, $n(\lambda)$, has several equations. Cauchy's equation, as given in Equation 2.4, is a much simpler approximation of the refractive index that remains very accurate at visible wavelengths.

$$n(\lambda) = A_C + \frac{B_C}{\lambda^2} + \frac{C_C}{\lambda^4} + \dots \tag{2.4}$$

Equation 2.4's $A_C, B_C, C_C, \dots$ variables are called the Cauchy coefficients and have known values dependent on the material. Taking only the first term of the derivative of the Cauchy equation allows us to approximate the angular dispersion of a prism.

$$\frac{d\theta}{d\lambda} = -\frac{B}{a}\frac{2B_C}{\lambda^3} \propto -\lambda^{-3} \tag{2.5}$$

Equation 2.5 shows that the angular dispersion of a prism is wavelength dependent and furthermore that longer wavelengths are dispersed less than shorter wavelengths (Birney et al., 2006; Hecht, 2017). The dependence of the angular dispersion, $d\theta/d\lambda$, on the wavelength, λ, is crucial for the formation of a spectrum but this cubic, non-linear, relation results in a non-linear spectrum. Since prisms rely on the refractive index of the material they are made of they have low angular dispersions.

Multiple prisms can be used to increase the angular dispersion but as the dispersion is non-linear it becomes increasingly more difficult to calibrate. The more material and material boundaries the light must pass through the more its intensity decreases due to attenuation effects and Fresnel losses. Even so, the transmittance of modern prisms for their selected wavelength range is generally very high due to improved manufacturing methods as well as improved transmitting materials.

The diffraction grating operates on the principle that when light interacts with a grating where the groove size is comparable to the light's wavelength, the light is dispersed as a function of its wavelength through constructive and destructive interference. This interference results in multiple diffracted beams m, called orders, either side of a central

reflected, or transmitted, beam such that $m \in Z$, where $m = 0$ is the non-dispersed, or reflected, beam.

$$m\lambda = \sigma(\sin(\alpha) \pm \sin(\beta)) \tag{2.6}$$

Equation 2.6 is referred to as the grating equation and its variables relate to Figure 2.3 such that m is the order of the diffracted beam being measured, λ is the wavelength of the incident light, σ is the groove spacing, α is the angle of incident light relative to the grating normal, and β is the angle of diffraction relative to the grating normal. It is important to note that the sign of α and β depend on whether the grating is reflective or tranmissive. In the case of a reflective grating, such as in Figure 2.3, the signs of α and β are the same relative to the grating normal, I.E. $\lambda = \sigma(\sin(\alpha) + \sin(\beta))$ for $m = 1$. In the case of a transmissive grating, the signs of α and β are the opposite relative to the grating normal, I.E. $\lambda = \sigma(\sin(\alpha) - \sin(\beta))$ for $m = 1$.

Equation 2.6 also describes how multiple wavelengths can share an angle of refraction when $m\lambda_m = (m + 1)\lambda_{m+1}$. The regions of an order that do not overlap with another order are called the free spectral range. To account for the overlaps and increase the free spectral range an order-blocking filter may be used, and the diffraction grating may be blazed by an angle, θ, such as in Figure 2.3. Blazing refers to the fact that the grooves on the surface of the grating are not symmetrical. The asymmetry of the grooves diffract the incident beam such that most of the incident beam's intensity is focused to a single order for a designated 'blazed' wavelength, λ_b.

$$m\lambda_b = 2\sigma \sin(\theta) \cos(\alpha - \theta) \tag{2.7}$$

where

$$2\theta = \alpha + \beta \tag{2.8}$$

Taking the derivative of Equation 2.6 with respect to λ and keeping α constant allows us to determine the angular dispersion of a diffraction grating.

$$\frac{d\beta}{d\lambda} = \frac{m}{\sigma \cos(\beta)} \tag{2.9}$$

Substituting m/σ with the grating equation gives

$$\frac{d\beta}{d\lambda} = \frac{\sin(\alpha) + \sin(\beta)}{\lambda \cos(\beta)} \propto \lambda^{-1} \tag{2.10}$$

Similarly to the dispersion of a prism, Equation 2.10 shows that the dispersion of a grating is wavelength dependent, but this dependence is only inversely proportional and thus more uniform across a wavelength range than that of a prism. Furthermore, shorter wavelengths are refracted less than longer wavelengths since there is no negative relation between the angular dispersion and the wavelength (Birney et al., 2006; Hecht, 2017).

As mentioned before, multiple subgroups exist for both dispersive prisms and diffractive gratings. For prisms, along with the single and multiple prism setups mentioned above, there also exist grisms and immersed gratings. A grism (Grating Prism) refers to a transmissive grating etched onto one of the transmissive faces of a prism and allows a single camera to capture both spectroscopic and photometric images without needing to

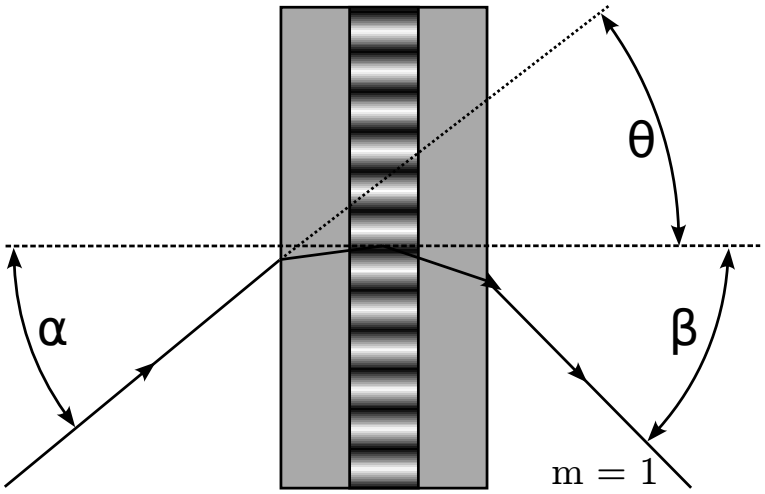

Figure 2.4: Geometry of a Volume Phase Holographic (VPH) grating for an incident monochromatic beam of light.

be moved, with and without the grism in the path of the beam of light, respectively. An immersed grating refers to a grism modified such that the transmissive grating is coated with reflective material. The primary source of dispersion for both grisms and immersive gratings is the grating and any aberration effects from the prism are negligible in comparison.

For gratings, along with transmissive and reflective gratings there also exist VPH gratings. A VPH grating consists of a photoresist, which is a light-sensitive material, sandwiched between two glass substrates. Diffraction is possible since the photoresist's refractive index varies near-sinusoidally perpendicularly to the gratings lines. This allows for sharper diffraction orders and low stray light scattering as compared to more traditional gratings but since blazing is not possible the efficiency is decreased. An echelle grating refers to two gratings set up such that the dispersed light from one is further diffracted by a second and allows for comparatively higher spectral resolutions when compared to more traditional grating setups. The gratings used as part of the echelle grating may be any type of dispersion element, but gratings are traditionally preferred due to the linearity of their resultant spectrum.

2.1.2 Detector and Spectroscopic Calibrations

Acquiring a spectrum from observations is more involved than simply reading out the data recorded on the CCD. A raw science image, which is the raw counts of the observed source read from the CCD with no calibrations applied, has on it a combination of useful science data as well as noise. The noise is a combination of random noise introduced through statistical processes and systematic noise introduced through the instrumentation and the observation conditions the source was observed under. This noise causes an uncertainty in the useful data and can be minimized, predominantly by calibrating for the systematic noise, but never fully removed (Howell, 2006).

The dominant source of noise in a raw image is detector noise. CCD's are manufactured to have a small base charge in each pixel, called the 'bias' current which allows the readout noise, a type of random noise, to better be sampled. There is also an unintentional

additional charge which is linearly proportional to the exposure time and originates from thermal agitation of the CCD material, called the 'dark' current. The dark current can be minimized and possibly ignored if the CCD is adequately cooled. These types of noise add to the charge held by a pixel and are thus considered additive.

The CCD is not a perfect detector and the efficiency of it and the optics of the telescope also contribute noise to the image. The efficiency of a CCD is referred to as the Quantum Efficiency, and it is a measure of what percentage of light striking the detector is actually recorded and converted to a charge. The efficiency of the CCD and telescope optics is also wavelength dependent and so the noise that results from them is more complex than that of additive noise. This type of noise is referred to as multiplicative noise.

Each image taken by a CCD will inherently have the additive types of noise in the image, and so bias and dark currents are the first types of noise to be accounted for by subtracting them from any subsequent images. Bias currents can be found by taking a bias image or by adding an overscan region to each image. A bias image is an image where the charges on the CCD are reset and then immediately read off without exposing anything on the detector, effectively taking an image with zero exposure time. Alternatively, to save time during an observational run, overscan regions may be added to the images. An overscan region refers to adding a few cycles to the readout of each column of the CCD such that the base current is read out and appended to each image.

Dark currents can be found by taking an image with nothing exposed onto the detector for a certain exposure time. This resultant dark image can then be scaled to the science images exposure time since the dark current is linearly proportional to exposure time. When the detector is capable of being held at precise temperatures, dark images may be taken over multiple hours during the day to produce a high quality master dark image that may then be scaled and subtracted from all subsequent images.

After the additive noise has been accounted for, the response from the pixels detecting the same incoming light are still not all the same due to the multiplicative noise which still needs to be accounted for. An image that has this noise accounted for is considered to be flat since all pixels share the same response to the incoming light. This noise can be measured by taking a 'flat' image, or alternatively a flat-field, and multiple types of flats can be taken which all in essence image a uniformly illuminated region to determine the pixel-to-pixel response.

Night sky flats are produced from science images where the images contain mostly sky. The science images are combined using the mode statistic which removes any celestial objects. This allows science images to be used for flat-fielding but at the cost of having a low Signal-to-Noise Ratio (S/N) because of the dim background sky. Dome flats are images taken of a flat surface inside the telescopes dome that has been uniformly and indirectly illuminated. These flats allow precise control of the light source and are also capable of being taken during the day. Finally, twilight flats are images taken of the twilight (or dawn) sky, when the Sun has just set, opposite the direction of the Sun at about 20° from zenith. Careful planning is required for twilight flats as the sky's brightness changes rapidly with the setting and rising of the Sun.

A flat-field must be normalized before being used to correct any science images since it only acts to account for the pixel-to-pixel response and not for the additive errors. The normalized flat image, $F^n_\lambda(x, y)$ can be calculated as:

$$F^n_\lambda(x,y) = \frac{F_\lambda(x,y) - B(x,y) - (\frac{t_S}{t_D})D(x,y)}{mode(F_\lambda(x,y) - B(x,y) - (\frac{t_S}{t_D})D(x,y))} \tag{2.11}$$

where $F_\lambda(x, y)$ is the non-corrected flat image, $B(x, y)$ is the bias image, $D(x, y)$ is the dark image which is scaled by t_S and t_D, the science image and dark image exposure times, respectively.

The calibrated science image, $S^*_\lambda(x, y)$, which accounts for the bias and dark currents as well as the flat fielding can then be calculated as:

$$S^*_\lambda(x,y) = \frac{S_\lambda(x,y) - B(x,y) - (\frac{t_S}{t_D})D(x,y)}{F^n_\lambda(x,y)}. \tag{2.12}$$

Multi-channel CCD's are detectors that use either multiple CCD's or a CCD with multiple output amplifiers which can be read out through multiple channels at the same time, increasing the detectors size while keeping the readout time constant. These CCD setups need additional calibrations, specifically cross-talk corrections and mosaicking.

Cross-talk noise refers to contamination that occurs during readout in one channel from another channel with a high signal and occurs because the signals can not be completely isolated from one another. Cross-talk corrections therefore account for this signal contamination between channels being read out at the same time (Freyhammer et al., 2001). Mosaicking is necessary for multi-channel CCD's since the digitized signal read out from the detector has no reference of the physical location of the pixel it was detected at. Mosaicking therefore orients the data acquired from a multi-channel detector correctly relatively to one another so that a single image is produced from the multiple channels read out from the detector.

Finally, calibrations necessary for spectroscopy are limited to wavelength calibrations. Since the dispersion element breaks the incident light into its constituent wavelengths non-linearly, as discussed in Section 2.1.1, the relation between the pixel on a detector and the wavelength of the light incident on it is unknown. Ideally, the spectrometer's optics would be modeled to produce a reliable pixel to wavelength calibration (see Eg. Liu and Hennelly, 2022), but this becomes increasingly more difficult for spectrometers with complex, non-sedentary, optical paths. Alternatively, a source with well-defined spectral features, with said features evenly populating the wavelength region of interest, such as in Figure 2.5 may be observed. The observed frame is commonly referred to as an 'arc' frame, after the arc lamps used to acquire the spectra, and should be observed alongside the science frames over the course of an observation run. It is important that the arc frame is observed at the same observing conditions and parameters as the science frames since the optical path will vary over the course of an observing run and for different observing parameters, invalidating previously acquired arc frames.

[1]NeAr plot sourced from `https://astronomers.salt.ac.za/data/salt-longslit-line-atlas/`

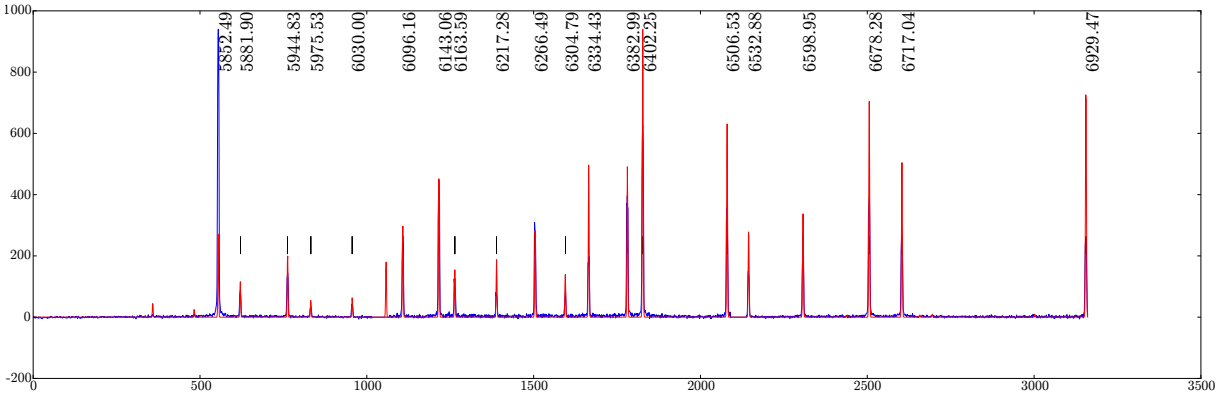

Figure 2.5: Example of an arc spectrum for NeAr taken with SALT's RSS using the PG1800 grating at a grating angle of 34.625°, an articulation angle of 69.258°, and covering a wavelength range of $\sim 5600 - 6900$Å. Plot adapted from SALT's published Longslit Line Atlases (as of 2023)[1]

The wavelength calibrations then consist of identifying a two dimensional pixel to wavelength conversion function from the arc frame which may later be applied to calibrate the science frames. The two most common approximations for wavelength calibrations are the Chebyshev and Legendre polynomial approximations as found in Equations 2.16 and 2.23, respectively. The Chebyshev polynomials are defined explicitly as:

$$T_n(x) = \cos(n \cos^{-1}(x)), \tag{2.13}$$

or recursively as:

$$\begin{aligned} T_0(x) &= 1 \\ T_1(x) &= x \\ T_n(x) &= 2xT_{n-1}(x) - T_{n-2}(x), \text{ for } n > 1 \end{aligned} \tag{2.14}$$

where T is a Chebyshev polynomial[2] of degree n. Chebyshev polynomials are orthogonal when weighted by $1/\sqrt{1-x^2}$, meaning that the inner product of any two different polynomials, $T_i(x)$ and $T_j(x)$, over the range of $[-1, 1]$ is zero.

$$\int_{-1}^{1} T_i(x) T_j(x) \frac{1}{\sqrt{1-x^2}}\, dx = \begin{cases} 0, & i \neq j \\ \pi/2, & i = j \neq 0 \\ \pi, & i = j = 0 \end{cases} \tag{2.15}$$

A one or two dimensional unknown calibration function may then be approximated by Chebyshev polynomials using:

$$f(x) \approx \sum_{i=0}^{N} c_i T_i(u) \tag{2.16}$$

or

$$F(x, y) \approx \sum_{i=0}^{N} \sum_{j=0}^{M} c_{ij} T_i(u) T_j(v), \tag{2.17}$$

[2]Denoted T as a hold-over from the alternate spelling, 'Tchebycheff'.

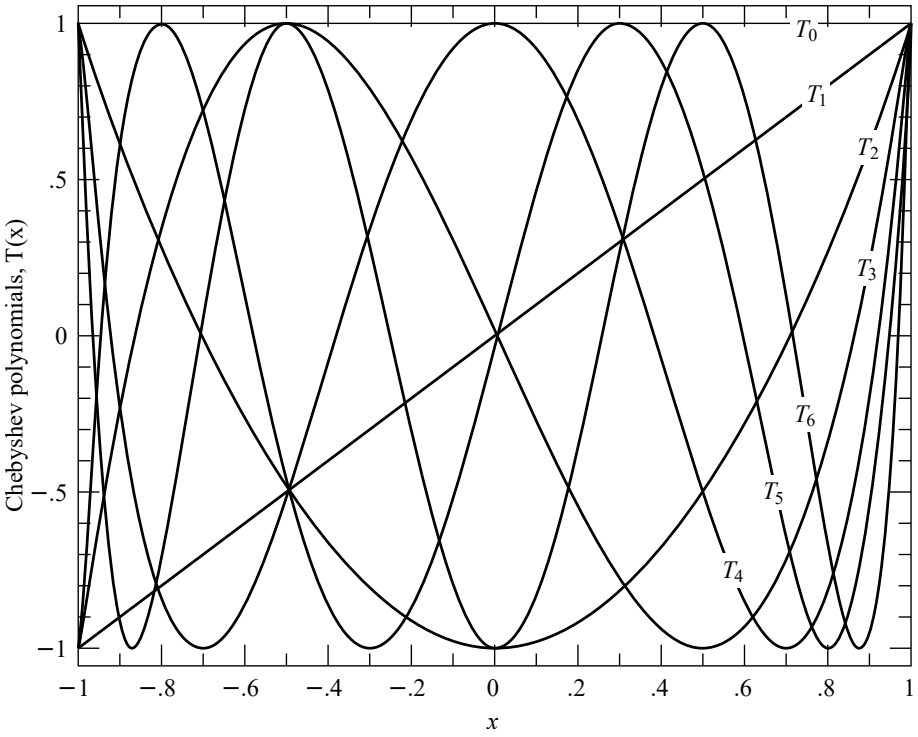

Figure 2.6: The first seven Chebyshev polynomials (T_0 through T_6) as defined by Equation 2.14 over the region $[-1, 1]$ for which they are orthogonal. Figure adapted from (Press et al., 2007) (2023)[3]

respectively, where N and M are the desired x and y orders, c_{ij} are the Chebyshev polynomial coefficients, and $u, v \in [-1, 1]$ are scaling factors to remap the variables $x, y \in [a, b]$ such that the orthogonality property of the Chebyshev polynomials holds true (Florinsky and Pankratov, 2015; Leng, 1997).

$$(u, v) = \frac{2(x, y) - a - b}{b - a} \qquad (x, y) = \frac{b - a}{2}(u, v) + \frac{a + b}{2} \tag{2.18}$$

The Chebyshev polynomials are more ideally suited for wavelength calibrations than standard polynomials since they are orthogonal and have minima and maxima located at $[-1, 1]$, as seen in Figure 2.6. This means that the chebyshev approximation is exact when $x = x_n$, where x_n are the positions of the $n-1$ x-intercepts of $T_N(x)$. This property greatly minimizes the error in the Chebyshev approximation, even at lower order approximations (Arfken and Weber, 1999).

$$x_n = \cos\left(\frac{\pi}{2}\frac{2n + 1}{N}\right) \tag{2.19}$$

Similar to the Chebyshev polynomials, the Legendre polynomials may be defined explicitly as:

$$P_n(x) = \frac{1}{2^n n!}\frac{d^n}{dx^n}(x^2 - 1)^n \tag{2.20}$$

or recursively as:

[3]Available digitally at numerical.recipes

$$\begin{aligned} P_0(x) &= 1 \\ P_1(x) &= x \\ P_n(x) &= \frac{2n+1}{n+1} x P_{n-1}(x) - \frac{n}{n+1} P_{n-2}(x), \text{ for } n > 1 \end{aligned} \tag{2.21}$$

where P is a Legendre polynomial of degree n. Legendre polynomials are also orthogonal over the range $[-1, 1]$.

$$\int_{-1}^{1} P_i(x) P_j(x)\, dx = \begin{cases} 0, & i \neq j \\ \frac{2}{2n+1}, & i = j \end{cases} \tag{2.22}$$

A one or two dimensional unknown calibration function may then be approximated by Legendre polynomials using:

$$f(x) \approx \sum_{n=0}^{N} a_n P_n(u) \tag{2.23}$$

or

$$F(x, y) \approx \sum_{i=0}^{N} \sum_{j=0}^{M} a_{ij} P_i(u) P_j(v), \tag{2.24}$$

respectively, where N and M are the desired x and y orders, u and v are the same mapping variable as in Equation 2.18, and a_{ij} are the Legendre polynomial coefficients. Legendre polynomials benefit from having the orthogonality condition with no weight necessary which makes their coefficients easier to compute but the error in a Legendre approximation of a function is greater than that of the error in a Chebyshev approximation for the same required order, N (in one dimension) (Ismail, 2005).

Regardless of which set of polynomials is chosen, the polynomials are fit to the known (wavelength, pixel) pair using a least squares method. The resultant minimized function may then be used to convert the science frames from a (x pixel, y pixel) coordinate system to a (wavelength, pixel) coordinate system.

2.2 Polarimetry

TODO: Origin of polarimetry (short history), and most important how polarimetry works in-depth (both practically and theoretically, I.E. Stokes parameters, wollaston prism, hwp, etc).

TODO: Uses and what its use in astrophysics is.

2.2.1 Polarimetric calibrations

TODO: Wollaston corrections and Tilt corrections

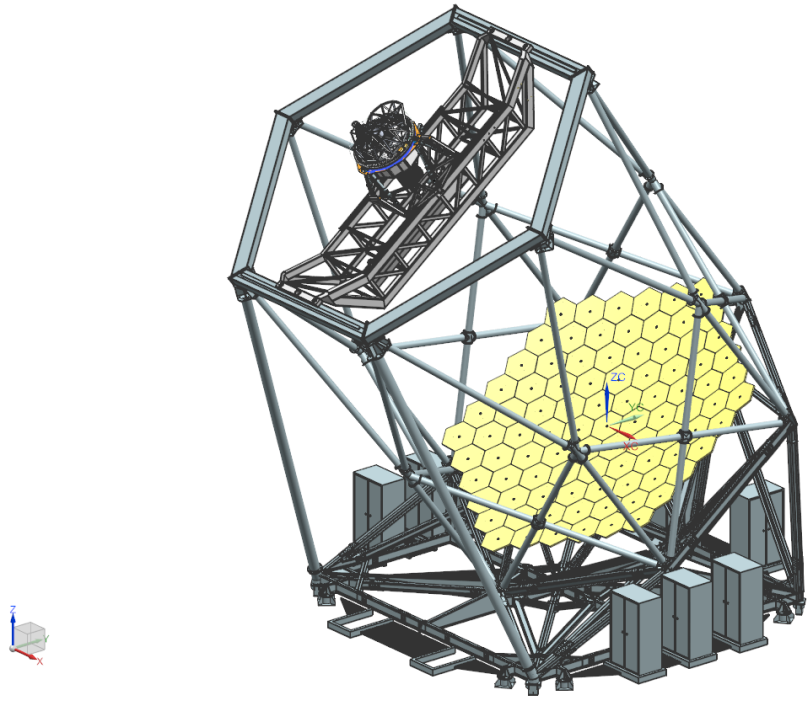

Figure 2.7: The tracker, supporting structure, and primary mirror of SALT. Figure adapted from the SALT call for proposals (2022)[4]

2.3 Spectropolarimetry

TODO: Origin of spectropolarimetry (short history), and most important how spectropolarimetry works in-depth (both practically and theoretically, I.E. frames, traces, O and E beams, etc).

TODO: Uses and what its use in astrophysics is.

2.4 The South African Large Telescope

SALT is a 10 m class optical/near-infrared telescope situated at the South African Astronomical Observatory (SAAO) field station near Sutherland, South Africa (Burgh et al., 2003). The operational design was based off of the Hobby-Eberly Telescope (HET) situated at McDonald Observatory, Texas, which limits the pointing of the telescope's primary mirror to a fixed elevation (37° from zenith in the case of SALT) while still allowing for full azimuthal rotation (Ramsey et al., 1998). Both SALT and HET utilise a spherical primary mirror which is stationary during observations and a tracker housing most of the instrumentation that tracks the primary mirrors spherically shaped focal path. Figure 2.7 depicts SALT's tracker (top left), supporting structure, and primary mirror (bottom right).

2.4.1 The primary mirror

The primary mirror is composed of 91 individual 1 m hexagonal mirrors which together form an 11 m segmented spherical mirror. Each mirror segment can be adjusted by actuators allowing the individual mirrors to approximate a single monolithic spherical

[4] `http://pysalt.salt.ac.za/proposal_calls/current/ProposalCall.html`

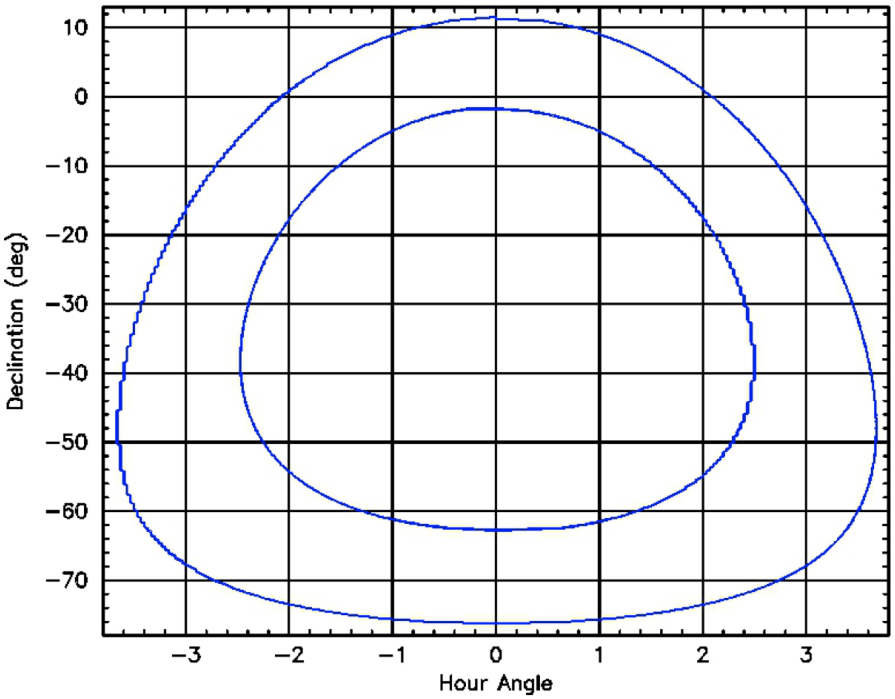

Figure 2.8: The visibility annulus of objects observable by SALT. Figure adapted from the SALT call for proposals (2013)[5]

mirror. The fixed elevation means that SALT's primary mirror has a fixed gravity vector allowing for a lighter, cost-effective supporting structure when compared to that of a more traditional altitude-azimuthal mount but with the trade-off that the control mechanism and tracking has increased complexity (Buckley et al., 2006).

2.4.2 Tracker and tracking

During observations the primary mirror is stationary and the tracker tracks celestial objects across the sky by moving along the primary focus. The tracker is capable of 6 degrees of freedom with an accuracy of 5 μm and is capable of tracking $\pm 6^\circ$ from the optimal central track position. Targets at declinations from 10.5° to -75.3°, as shown in Figure 2.8 are accessible during windows of opportunity. As the tracker moves along the track the effective collecting area varies and thus SALT has a varying effective diameter of 7 m to 9 m when the tracker is furthest and closest to the optimal central position, respectively.

The tracker is equipped with a 4 mirror spherical aberration corrector (O'Donoghue, 2000), and an atmospheric dispersion compensator (O'Donoghue, 2002), which corrects for the spherical aberration caused by the geometry of the primary mirror and allows access to wavelengths as short as 3200 Å. These return a corrected flat focal plane with an $8'$ diameter field of view at prime focus on to the science instruments, with a $1'$ annulus around it used by the Tracker in a closed-loop guidance system.

[5] `https://pysalt.salt.ac.za/proposal_calls/2013-2/`

2.4.3 The Robert Stobie Spectrograph

SALT is equipped with the SALT Imaging Camera (SALTICAM) and the RSS science instruments onboard the tracker, and the High Resolution Spectrograph (HRS) and Near Infra-Red Integral Field Spectrograph (NIR IFS) science instruments which are fibre-fed from the tracker to their own climate controlled rooms. The RSS is the most used instrument on SALT and the only instrument used for spectropolarimetry, and as such will be discussed in more depth than the other instruments.

The NIR IFS is currently being commissioned and will extend SALT's operational wavelength range from 3200 - 9000 Å to 3200 - 17000 Å, providing medium resolution spectroscopy at R = 2000 - 5000 over NIR wavelengths (Brink et al., 2022; Wolf et al., 2022). This is ideally suited for studies of nearby galaxies.

The HRS echelle spectrograph was designed for high resolution spectroscopy at R = 37000 - 67000 covering a wavelength range of 3700 - 8900 Å and consists of a dichroic beam splitter and two VPH gratings (Nordsieck et al., 2003). This instrument is capable of stellar atmospheric and radial velocity analysis.

The SALTICAM functions as the acquisition camera and simple science imager with various imaging modes, such as full-mode and slot-mode imaging, and supports low exposure times, down to 50 ms (O'Donoghue et al., 2006). This enables photometry of faint objects, especially at fast exposure times.

The RSS functions as the primary spectrograph on SALT and can operate in long-slit spectroscopy and spectropolarimetry modes, narrowband imaging mode, multi-object and high resolution spectroscopy modes, and low resolution Fabry-Pérot imaging spectroscopy and tunable filter narrowband imaging modes (for an in-depth discussion on operational modes see Kobulnicky et al., 2003).

TODO: Optical layout (Figure) and description, and CCD/Lamps/Filters etc. available. Focus on spectropolarimetry and a short description on how observations are organized, gratings, spectral ranges, as well as the latest developments (PG0700, and anything else new)

2.5 RSS Spectropolarimetric Reductions

TODO: How spectropolarimetry reductions differ from spectroscopy, polarimetry, and general spectropolarimetry reductions

2.5.1 General Reduction Process

TODO: How reductions would be done in general and through pure IRAF.

I.E. Frames observed → flat, bias, arc, multiple targets, others(?)

Corrections → flat fielding, bias subtraction (eq from obs. astro), others(?)

Calibrations → wavelength, flux, shifting (trace to centre), background subtraction, others(?)

Extraction → spectral extraction, others(?)

~~Stokes parameter calculations / Post processing / Displaying / saving / comparing results~~

2.5.2 POLSALT

TODO:

In depth but not a users guide, more focus on purpose than the parameters (I.E. why each step is necessary and draw comparison to general reduction)

Why polsalt works without any major need for concern.) "All steps except for the wavelength calibration and spectral extraction run with no user input. The spectral extraction is not a calibration but a simple check to make sure the entire trace is included in the window and also that the background regions do not contain any other objects lying on the frame or include the trace."

Raw image reductions

[Bias/Dark/Flat/Fringe(?)/Crosstalk/Mosaicking] All processes run / files created / PURPOSE!

Wavelength calibrations

[Arc/Background subtraction/Cosmic ray rejection] All processes run / files created / PURPOSE! / Heavy focus since supplementary pipeline replaces this step

Spectral extraction

All processes run / files created / PURPOSE!

Raw Stokes calculations

[Wollaston] All processes run / files created / PURPOSE!

Final Stokes calculations

All processes run / files created / PURPOSE!

Post processing analysis

PURPOSE Data Culling (BASH) (not used but mention use) / Flux Calibrations (BASH and errors in GUI (make 100% sure about division error and notify Danielle before/if planning on including)) / saving plot and text pipeline results (BASH and GUI) / Synthetic Filtering (BASH) /

Mention bash script and GUI versions and differences, as well as what SALT's preferred method is

Chapter 3

Developed Tools

TODO: This chapter is **highly** in depth as it is the 'meat' of the dissertation

3.1 Limitations of POLSALT and the Need for a Supplementary Tool

TODO: Shortcomings (bad word - must change)/limitations of polsalt **in depth**, can mention other faults very briefly but the main take away should be the need for a way to do the wavelength calibration with more control as well as the need to check the beam (and target frame) wavelength calibrations against one another (since very accurate wavelength calibration necessary for stokes parameter calculations)

Why an external supplementary tool necessary (and how it overcomes POLSALTS limitations) and benefit of it over trying to 'brute force' polsalt reductions

3.2 Wavelength calibrations using the Supplementary Pipeline and IRAF

TODO: short description of what is to be discussed

3.2.1 Splitting the uncalibrated wavelength files

TODO: All processes run in pipeline split Focus on **why**. Parsing polsalt mxgbp frame into something useable by IRAF and making sure the header reflects the changes

3.2.2 IRAF wavelength calibration

TODO: All wavelength calibration steps - Again, focus on **why** instead of how

Identify

Reidentify

Fitcoords

(Optional) Transform (mention good for sanity checks which is not possible using the pure polsalt implementation)

3.2.3 Joining the wavelength calibrated files

TODO: All processes run in pipeline join. Focus on **why**. Parsing IRAF frames to be used by POLSALT and making sure the header and extensions reflect the changes

3.3 Additional Tools

3.3.1 Cross correlation

TODO: Why a cross correlation necessary and how it works

3.3.2 Skyline comparisons

TODO: Again, why a skyline comparison necessary and how it works. Also how the frame is transformed (IRAF bypassed) and that the flux is not conserved so only for checking and not for science use.

3.4 General Reduction Procedure

TODO: General reduction procedure from raw data to finalized results

This includes POLSALT pre-reductions, splitting, IRAF wavelength calibrations, checking, joining, and POLSALT finalizations. (Include Relative flux calibrations for 'shape correcting' spectrum??)

Chapter 4

Testing

TODO: Add all tests done and comparisons.

- 3C 279 - 4C+01.02 - David data (not in next section publications because still during pipeline development. Reductions done through polsalt, but after publication used as preliminary testing data)

Chapter 5

Science Applications

TODO: short introduction to chapter contents

5.1 Application to Spectropolarimetric Standards

TODO: Spectropolarimetric standards (4 highly polarised, 2 non-polarised)
- Background on objects
- Reductions
- Actual results - comparison of polsalt results to supplementary pipeline results
- Science results, what the results can tell us and why it is useful, also comparison of results to FORS1/2 published data, focus on the polarisation results

5.2 Application in publications

TODO: Summary of results from papers in appendix.
- Hester paper(s)
- Joleen proceedings and work
- My proceedings

TODO: 3C 279 and 4C+01.02

Give Background on objects, Reduction steps, and Science results (what the results can tell us and why it is useful)

(comparison of polsalt results to supplementary pipeline results will be in testing)

Chapter 6

Conclusions

TODO: A summary of the dissertation, main focus on the results and that the supplementary pipeline is a success since it allows an alternate method using IRAF to wavelength calibrate the polsalt data.

Acknowledgements

I hereby acknowledge and express my sincere gratitude to the following parties for their valuable contributions:

- TODO: Add acknowledgements!

List of Acronyms

ADC	Analog-to-Digital Converter
CCD	Charged-Coupled Device
CMOS	Complementary Metal-Oxide-Semiconductor
HET	Hobby-Eberly Telescope
HRS	High Resolution Spectrograph
NIR IFS	Near Infra-Red Integral Field Spectrograph
RSS	Robert Stobie Spectrograph
S/N	Signal-to-Noise Ratio
SAAO	South African Astronomical Observatory
SALT	South African Large Telescope
SALTICAM	SALT Imaging Camera
VPH	Volume Phase Holographic

Bibliography

George B. Arfken and Hans J. Weber. Mathematical methods for physicists, 1999.

D. Scott Birney, Guillermo Gonzalez, and David Oesper. Observational Astronomy - 2nd Edition. Cambridge University Press, 2006. doi: 10.2277/0521853702.

Janus D. Brink, Moses K. Mogotsi, Melanie Saayman, Nicolaas M. Van der Merwe, Jonathan Love, and Alrin Christians. Preparing the SALT for near-infrared observations. In Heather K. Marshall, Jason Spyromilio, and Tomonori Usuda, editors, Ground-based and Airborne Telescopes IX, volume 12182 of Society of Photo-Optical Instrumentation Engineers (SPIE) Conference Series, page 121822E, August 2022. doi: 10.1117/12.2627328.

David A. H. Buckley, Gerhard P. Swart, and Jacobus G. Meiring. Completion and commissioning of the Southern African Large Telescope. In Larry M. Stepp, editor, Society of Photo-Optical Instrumentation Engineers (SPIE) Conference Series, volume 6267 of Society of Photo-Optical Instrumentation Engineers (SPIE) Conference Series, page 62670Z, June 2006. doi: 10.1117/12.673750.

Christian Buil. CCD astronomy : construction and use of an astronomical CCD camera / Christian Buil ; translated and adapted from the French by Emmanuel and Barbara Davoust. Willmann-Bell, Richmond, Va, 1st english ed. edition, 1991. ISBN 0943396298.

Eric B. Burgh, Kenneth H. Nordsieck, Henry A. Kobulnicky, Ted B. Williams, Darragh O'Donoghue, Michael P. Smith, and Jeffrey W. Percival. Prime Focus Imaging Spectrograph for the Southern African Large Telescope: optical design. In Masanori Iye and Alan F. M. Moorwood, editors, Instrument Design and Performance for Optical/Infrared Ground-based Telescopes, volume 4841 of Society of Photo-Optical Instrumentation Engineers (SPIE) Conference Series, pages 1463–1471, March 2003. doi: 10.1117/12.460312.

Marshall H. Cohen. Genesis of the 1000-foot Arecibo dish. Journal of Astronomical History and Heritage, 12(2):141–152, July 2009.

Königlich Bayerische Akademie der Wissenschaften. Denkschriften der Königlichen Akademie der Wissenschaften zu München für das Jahre 1820 und 1821, volume 8. Die Akademie, 1824. URL `https://books.google.co.za/books?id=k-EAAAAAYAAJ`.

I. V. Florinsky and A. N. Pankratov. Digital terrain modeling with the chebyshev polynomials. Machine Learning and Data Analysis, 1(12):1647 – 1659, 2015. doi: 10.48550/ARXIV.1507.03960. URL `https://arxiv.org/abs/1507.03960`.

L. M. Freyhammer, M. I. Andersen, T. Arentoft, C. Sterken, and P. Nørregaard. On Cross-talk Correction of Images from Multiple-port CCDs. Experimental Astronomy, 12(3):147–162, January 2001. doi: 10.1023/A:1021820418263.

E. Hecht. Optics. Pearson Education, Incorporated, 2017. ISBN 9780133977226. URL https://books.google.co.za/books?id=ZarLoQEACAAJ.

Steve B. Howell. Handbook of CCD Astronomy, volume 5. Cambridge University Press, 2006.

Mourad E. H. Ismail. Classical and Quantum Orthogonal Polynomials in One Variable. Encyclopedia of Mathematics and its Applications. Cambridge University Press, 2005. doi: 10.1017/CBO9781107325982.

James Janesick, James T. Andrews, and Tom Elliott. Fundamental performance differences between CMOS and CCD imagers: Part 1. In David A. Dorn and Andrew D. Holland, editors, Society of Photo-Optical Instrumentation Engineers (SPIE) Conference Series, volume 6276 of Society of Photo-Optical Instrumentation Engineers (SPIE) Conference Series, page 62760M, June 2006. doi: 10.1117/12.678867.

G. Kirchhoff and R. Bunsen. Chemische Analyse durch Spectralbeobachtungen. Annalen der Physik, 189(7):337–381, January 1861. doi: 10.1002/andp.18611890702.

Henry A. Kobulnicky, Kenneth H. Nordsieck, Eric B. Burgh, Michael P. Smith, Jeffrey W. Percival, Ted B. Williams, and Darragh O'Donoghue. Prime focus imaging spectrograph for the Southern African large telescope: operational modes. In Masanori Iye and Alan F. M. Moorwood, editors, Instrument Design and Performance for Optical/Infrared Ground-based Telescopes, volume 4841 of Society of Photo-Optical Instrumentation Engineers (SPIE) Conference Series, pages 1634–1644, March 2003. doi: 10.1117/12.460315.

Gerard Leng. Compression of aircraft aerodynamic database using multivariable chebyshev polynomials. Advances in Engineering Software, 28(2):133–141, 1997. ISSN 0965-9978. doi: https://doi.org/10.1016/S0965-9978(96)00043-9. URL https://www.sciencedirect.com/science/article/pii/S0965997896000439.

Dongyue Liu and Bryan M. Hennelly. Improved wavelength calibration by modeling the spectrometer. Applied Spectroscopy, 76(11):1283–1299, 2022. doi: 10.1177/00037028221111796. URL https://doi.org/10.1177/00037028221111796. PMID: 35726593.

I. Newton and W. Innys. Opticks:: Or, A Treatise of the Reflections, Refractions, Inflections and Colours of Light. Opticks:: Or, A Treatise of the Reflections, Refractions, Inflections and Colours of Light. William Innys at the West-End of St. Paul's., 1730. URL https://books.google.co.za/books?id=GnAFAAAAQAAJ.

Kenneth H. Nordsieck, Kurt P. Jaehnig, Eric B. Burgh, Henry A. Kobulnicky, Jeffrey W. Percival, and Michael P. Smith. Instrumentation for high-resolution spectropolarimetry in the visible and far-ultraviolet. In Silvano Fineschi, editor, Polarimetry in Astronomy, volume 4843 of Society of Photo-Optical Instrumentation Engineers (SPIE) Conference Series, pages 170–179, February 2003. doi: 10.1117/12.459288.

D. O'Donoghue, D. A. H. Buckley, L. A. Balona, D. Bester, L. Botha, J. Brink, D. B. Carter, P. A. Charles, A. Christians, F. Ebrahim, R. Emmerich, W. Esterhuyse, G. P. Evans, C. Fourie, P. Fourie, H. Gajjar, M. Gordon, C. Gumede, M. de Kock, A. Koeslag, W. P. Koorts, H. Kriel, F. Marang, J. G. Meiring, J. W. Menzies, P. Menzies, D. Metcalfe, B. Meyer, L. Nel, J. O'Connor, F. Osman, C. Du Plessis, H. Rall, A. Riddick, E. Romero-Colmenero, S. B. Potter, C. Sass, H. Schalekamp, N. Sessions, S. Siyengo, V. Sopela, H. Steyn, J. Stoffels, J. Scholtz, G. Swart, A. Swat, J. Swiegers, T. Tiheli, P. Vaisanen, W. Whittaker, and F. van Wyk. First science with the Southern African Large Telescope: peering at the accreting polar caps of the eclipsing polar SDSS J015543.40+002807.2. MNRAS, 372(1):151–162, October 2006. doi: 10.1111/j.1365-2966.2006.10834.x.

Darragh O'Donoghue. Correction of spherical aberration in the Southern African Large Telescope (SALT). In Philippe Dierickx, editor, Optical Design, Materials, Fabrication, and Maintenance, volume 4003 of Society of Photo-Optical Instrumentation Engineers (SPIE) Conference Series, pages 363–372, July 2000. doi: 10.1117/12.391526.

Darragh O'Donoghue. Atmospheric dispersion corrector for the Southern African Large Telescope (SALT). In Richard G. Bingham and David D. Walker, editors, Large Lenses and Prisms, volume 4411 of Society of Photo-Optical Instrumentation Engineers (SPIE) Conference Series, pages 79–84, February 2002. doi: 10.1117/12.454874.

W. H. Press, S. A. Teukolsky, W. T. Vetterling, and B. P. Flannery. Numerical Recipes 3rd Edition: The Art of Scientific Computing. Cambridge University Press, 2007. ISBN 9780521880688. URL `https://books.google.co.za/books?id=1aAOdzK3FegC`.

Lawrence W. Ramsey, M. T. Adams, Thomas G. Barnes, John A. Booth, Mark E. Cornell, James R. Fowler, Niall I. Gaffney, John W. Glaspey, John M. Good, Gary J. Hill, Philip W. Kelton, Victor L. Krabbendam, L. Long, Phillip J. MacQueen, Frank B. Ray, Randall L. Ricklefs, J. Sage, Thomas A. Sebring, W. J. Spiesman, and M. Steiner. Early performance and present status of the Hobby-Eberly Telescope. In Larry M. Stepp, editor, Advanced Technology Optical/IR Telescopes VI, volume 3352 of Society of Photo-Optical Instrumentation Engineers (SPIE) Conference Series, pages 34–42, August 1998. doi: 10.1117/12.319287.

Stephen F. Tonkin. Practical Amateur Spectroscopy. The Patrick Moore Practical Astronomy Series. Springer London, 2013. ISBN 9781447101277. URL `https://books.google.fr/books?id=b2fgBwAAQBAJ`.

Marsha J. Wolf, Matthew A. Bershady, Michael P. Smith, Kurt P. Jaehnig, Jeffrey W. Percival, Joshua E. Oppor, Mark P. Mulligan, and Ron J. Koch. Laboratory performance and commissioning status of the SALT NIR integral field spectrograph. In Christopher J. Evans, Julia J. Bryant, and Kentaro Motohara, editors, Ground-based and Airborne Instrumentation for Astronomy IX, volume 12184 of Society of Photo-Optical Instrumentation Engineers (SPIE) Conference Series, page 1218407, August 2022. doi: 10.1117/12.2630242.

William H. Wollaston. XII. A Method of Examining Refractive and Dispersive Powers, by Prismatic Reflection. Philosophical Transactions of the Royal Society of London Series I, 92:365–380, January 1802. doi: 10.1098/rstl.1802.0013.